Electrostatic potential calculations for whole-volume gyrokinetic modeling of stellarators

T. Moritaka[1,2], M. Cole[3], R. Hager[3], S. Ku[3], C-S. Chang[3], S. Ishiguro[1,2]

[1] *National Institute for Fusion Science, Toki 509-5292, Japan*

[2] *The Graduate University for Advanced Studies, SOKENDAI, Toki, 509-5292, Japan*

[3] *Princeton Plasma Physics Laboratory, New Jersey 08540, USA*

The gyrokinetic model has been widely employed for kinetic plasma simulations on turbulent and neoclassical transport phenomena in magnetic confinement devices. Flux coordinates are suitable to take field line structures into account in solving gyrokinetic equations inside the last closed flux surface. On the other hand, the gyrokinetic particle-in-cell code, X-point Gyrokinetic Code (XGC)[1], which is developed for whole-volume modeling of Tokamaks, utilizes finite element method and unstructured mesh. The unstructured mesh is generated based on the flux function to cover the entire region inside the vacuum vessel. This paper briefly presents new numerical techniques developed to extend XGC for stellarators, namely XGC-S[2, 3, 4, 5].

We first summarize the difficulties to extend the gyrokinetic particle-in-cell code for whole-volume gyrokinetic modeling of stellarators. The main difficulties come from the finite-element field solver in the complicated magnetic field in the edge region. The field equation considered here is

$$-\nabla_\perp \cdot \frac{n_0 m}{e\mathrm{B}^2}\nabla_\perp \Phi + n_0 \frac{\delta\Phi}{T_e} = \tilde{n}, \tag{1}$$

$$\delta\Phi = \Phi - \langle\Phi\rangle, \tag{2}$$

where n_0, T_e, Φ and $\tilde{n}$ are equilibrium density and electron temperature, electrostatic potential and density perturbation, respectively. $\langle\rangle$ and $\nabla_\perp$ stand for flux-average and perpendicular gradient operators. This equation is used for electrostatic perturbation with a relatively long wavelength assuming adiabatic electron response. Specific difficulties may be as follows. (A) Flux functions and coordinates are not defined there. Therefore we should generate unstructured meshes without using them. (B) The flux-average operator in the field equation should be applied to the entangled field lines. (C) Magnetic field lines may direct significantly away from the toroidal direction. In this case, the toroidal cross-sections are not effective to define the gradient operator. Similar difficulties would arise in more general expressions of gyrokinetic field equation.

Unstructured meshes with vertices following magnetic field lines are appropriate for particle-mesh interpolation without numerical diffusion across magnetic field lines. We can generate

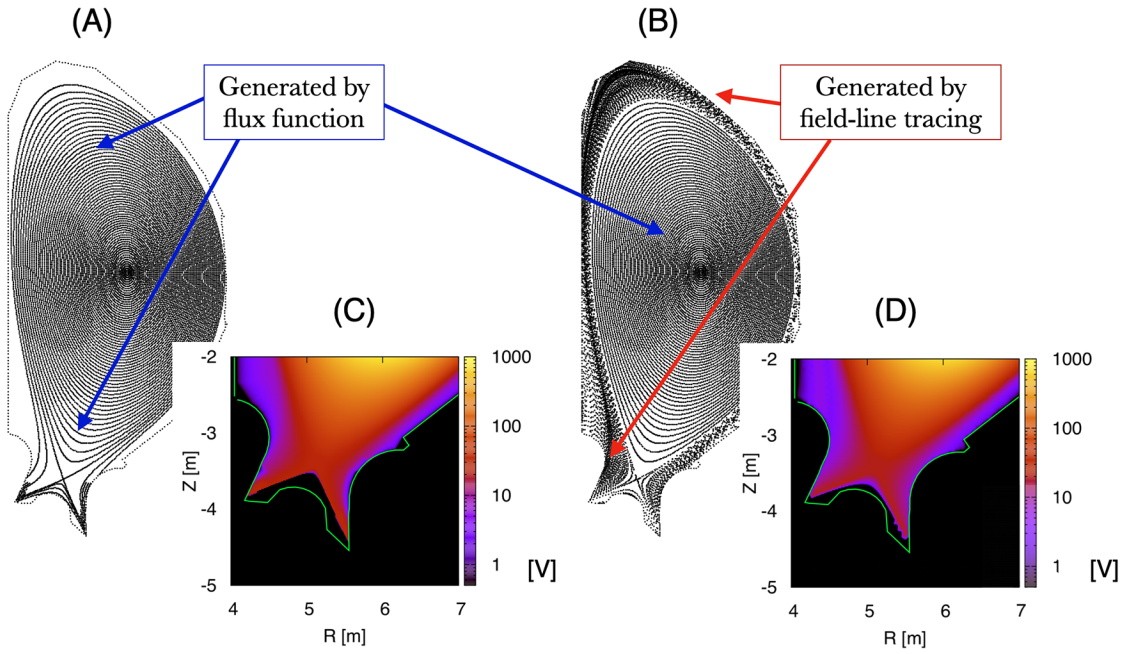

Figure 1: Two unstructured meshes in the ITER equilibrium generated based on (A) the flux function (core + edge), and (B) field line tracing (edge) and the flux function (core). (C), (D) Potential profiles near the divertor resulting from these two meshes, (A) and (B), respectively.

such meshes for three dimensional VMEC equilibria of stellarators based on flux coordinates. This method is not applicable to the edge regions because flux coordinates are not defined. Alternatively the mesh vertices can be defined by using numerical field line tracing[2]. Crossing points between magnetic field lines and a surface are connected with each other to define triangle elements. We test this method using a magnetic equilibrium of ITER including the edge region. Electrostatic potentials are calculated by using two different unstructured meshes. One is generated by the original method using flux function for whole-volume modeling of tokamaks. The other is generated by the present (edge region) and the original (core region) methods. Figure 1 (A) and (B) show distributions of triangle vertices in these two meshes. Resulting potential profiles are shown in Fig. 1 (C) and (D). While mesh structures are quite different, similar potential profiles are obtained even in the divertor region.

The flux-average operator is given by a dense matrix in the field equation. Therefore standard matrix solvers such as preconditioned conjugate gradient method are not sufficient to obtain the solution. The solution is obtained by iteratively solving the modified equation,

$$-\nabla_\perp \cdot \frac{n_0 m}{eB^2}\nabla_\perp \delta\Phi^{n+1} + \frac{n_0}{T_e}\delta\Phi^{n+1} = n + \nabla_\perp \cdot \frac{n_0 m}{eB^2}\nabla_\perp \langle\Phi^n\rangle, \tag{3}$$

where n is the iteration index. For given $\langle\Phi^n\rangle$, this is a linear equation with a sparse matrix. However the iteration on n is not sufficiently converged especially in non-axisymmetric geome-

tries. In order to reduce numerical cost of this calculation, we have improved the field solver using expansions of potential and density by magnetic fluxes,

$$\langle \Phi \rangle = \sum_{m}^{M} \Phi_m \langle I \rangle_m, \qquad \langle n \rangle = \sum_{m}^{M} n_m \langle I \rangle_m, \tag{4}$$

where m, M, Φ_m and n_m are index of flux, total number of flux and expansion coefficients of potential and density, respectively. $\langle I \rangle_m$ represents the unit profile uniformly distributed along the $m-th$ magnetic flux. We prepare solutions for density profiles $\langle I \rangle_m$ before time step calculations. In the time step cycles, we can obtain general solutions including fluctuation components, $\langle \Phi \rangle + \delta\Phi$, using linear combination of the prepared solutions and a few calculations solving linear equations with sparse matrices[6].

The perpendicular gradient operator, $\nabla_\perp$, should be defined on a plane perpendicular to the equilibrium magnetic field. The toroidal cross section is approximately perpendicular to magnetic field lines in the core region. Therefore unstructured mesh on the toroidal cross section would be suitable for this region. If magnetic field lines direct away from the toroidal direction, we need to construct curved planes perpendicular to the field lines to apply a two-dimensional finite-element method to the field equation. This problem is important in stellarators such as Large Helical Device where magnetic field lines direct to divertors between two helical coils. We construct the curved surfaces for Large Helical Device by means of a numerical optimization technique. The surfaces are defined in the helical coordinates by functions $\phi = \phi(R,Z)$, where ϕ is the toroidal angle. Constant $\phi(R,Z)$ indicates the toroidal cross sections. The optimized $\phi(R,Z)$ is calculated by the steepest descent method. Here the evaluation function is given by the angles between the plane normal vector at discretized mesh points on (R,Z) and magnetic field lines. Figure 2 (A) and (B) show the optimized surface in the helical coordinates[6]. Color contour indicates the values of the evaluation function, $E_{m,n} = |\hat{n} \cdot \mathbf{B}|/|B|$, where $\hat{n}$ and (m,n) are plane normal and index of mesh point on (R,Z), respectively. $E_{m,n} \sim 1$ means the surface is approximately perpendicular to the magnetic field line around the mesh point. Figure 2 (C) and (D) show bird's-eye views of the optimized surface in Cartesian coordinates[6]. The optimized surface is similar to the toroidal cross section inside the last closed flux surface (orange), and twisted along the vacuum vessel (blue) outside the last closed flux surface.

In this paper, we briefly introduce basic numerical techniques developed toward whole-volume modeling of stellarators. The main difficulties are related to solving the field equation, i.e., gyrokinetic Poisson equation, in complicated field line structures in the edge region of stellarators. The present numerical techniques are relevant to unstructured mesh generation and sufficient field solver with a finite-element method in this region. XGC-S has been employed

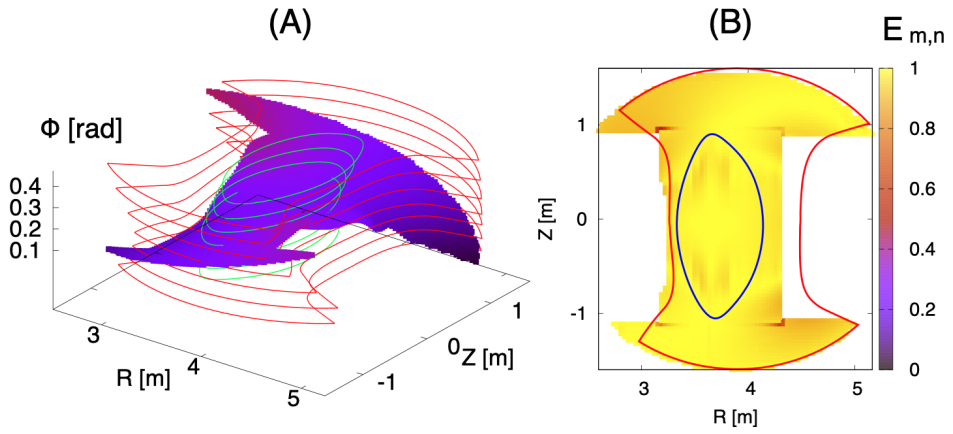

Figure 2: (A) Optimized surface with $\phi = (2\pi/36)/N_{turn}/36$ at the magnetic axis in the helical coordinates, where $N_{turn} = 10$ is the toroidal periodicity of Large Helical Device. (B) Value of the evaluation function $E = |\hat{n} \cdot \mathbf{B}|/|B|$ as a function of (R, Z)[6].

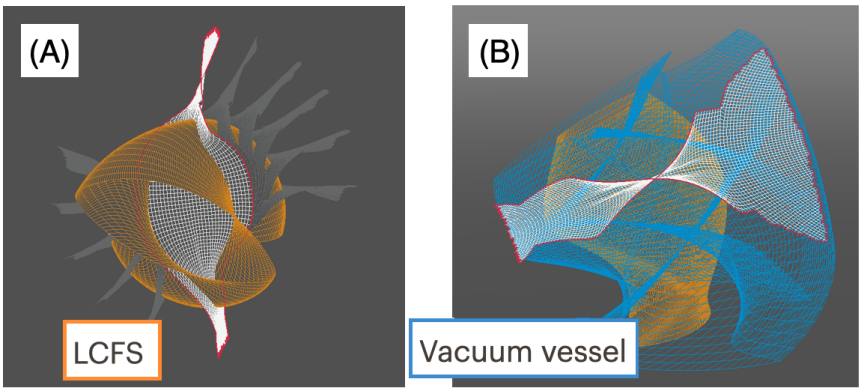

Figure 3: Optimized surfaces in Cartesian coordinates. (A) Bird's-eye view in the toroidal direction. (B) Bird's-eye view from the upward direction. Orange and blue surfaces indicate the last closed flux surface and the vacuum vessel[6].

for linear and non-linear simulations of ion temperature gradient modes in the core region of stellarators[3, 4, 5] and high-energy particle orbit simulations in the entire region of Large Helical Device[2]. We will implement these techniques to XGC-S for self-consistent gyrokinetic simulations including the edge region of stellarators in the future.

References

[1] S. Ku, C. S. Chang, R. Hager et al., Phys. Plasmas **25**, 056107 (2018).

[2] T. Moritaka, R. Hager, M. Cole et al., Plasma, **2** 179-200 (2019).

[3] M. D. J. Cole, R. Hager, T. Moritaka et al., Phys. Plasmas, **26** 082501 (2019).

[4] M. D. J. Cole, T. Moritaka, R. Hager et al., Phys. Plasmas, **27** 044501 (2019).

[5] M. Cole, T. Moritaka, R. Hager et al., Phys. Plasmas **27** 044501 (2020).

[6] T. Moritaka, M. Cole, R. Hager et al, Plasma and Fusion Res. **6**, 2403054 (2021).